Met. Mater. Int., Vol. 22, No. 1 (2016), pp. 12~19
doi: 10.1007/s12540-015-5515-2

Modeling and Experimental Verification for Non-Equibiaxial Residual Stress Evaluated by Knoop Indentations

Young-Cheon Kim[1], Hee-Jun Ahn[2], Dongil Kwon[2], and Ju-Young Kim[1,3,*]

[1]School of Materials Science and Engineering, UNIST (Ulsan National Institute of Science and Technology), Ulsan 44919, Korea
[2]Department of Materials Science and Engineering, Seoul National University, Seoul 08826, Korea
[3]KIST-UNIST Ulsan Center for Convergent Materials, UNIST, Ulsan 44919, Korea

(received date: 16 September 2015 / accepted date: 18 October 2015)

Surface residual stress is usually characterized by two parameters; (1) magnitude and (2) direction of two principal residual stresses. We propose a novel way to evaluate these parameters by instrumented indentation testing (IIT) using a Knoop indenter, which has two-fold symmetry. Non-equibiaxial surface stress causes a shift from residual stress in the force-indentation depth curve of IIT that depends on the Knoop indentation in-plane angle between residual stress and long diagonal of Knoop indenter. We develop a theoretical model to evaluate surface residual stress using only experimental parameters obtained by four Knoop IITs at 45° rotated angles, by introducing mathematical definition of conversion factor, α, which ratio of normal and parallel conversion factors was known as constants (~0.34) on previous studies. We verify this model by Knoop IITs on four metallic cruciform samples in which the surface residual stress is controlled by bending. Experimental results of principal stress and direction show good agreements with applied stress and directions.

Keywords: residual stress, indentation, metals, surface, Knoop indenter

1. INTRODUCTION

Instrumented indentation testing (IIT) is a useful tool for evaluating surface residual stress in a non-destructive way. Fundamental idea is that the curve of force versus indentation depth is shifted upward by compressive surface residual stress and downward by tensile surface residual stress compared to the stress-free state, and that the amount of residual stress is approximately proportional to the force change ΔL at a given indentation depth (Fig. 1) [1-3]. For tensile residual stress, it takes less force to attain a certain indentation depth than in the stress-free state since the residual stress stretches materials along in-plane directions, while compressive residual stress pushes the indenter out so that a greater force is necessary to attain a certain indentation depth.

Early approaches to evaluating surface residual stress using hardness testing were to correlate hardness values and the amount of surface residual stress. Sines and Carlson [4] controlled residual stress at the surface of metallic materials by bending and found that the difference in Rockwell hardness depended on the magnitude and direction of the residual stress. Later, it was reported that hardness in IIT is independent of residual stress [5-7]. The definitions of conventional hardness and IIT hardness are different [8], so this issue can be controversial. Frankel *et al*. [9] related the quantitative effect of residual stress on indentation yielding by stress-sensitive behavior to Rockwell hardness.

Concurrently with the development of nanoindentation, many studies evaluating surface residual stress using nanoindentation were made [10,11]. Tsui *et al*. [6], studying the influence of in-plane stress on indentation plasticity, reported that hardness is invariant regardless of residual stress in the elastic deformation regime. Finite element analysis (FEA) results [5,6] also supported the finding that IIT hardness is insensitive to residual stress. IIT hardness is defined as the maximum applied force over the contact area in the loaded state: $H = L_{max}/A_c$. As shown in Fig. 2, tensile residual stress introduces sink-in, reducing the contact area from that in the stress-free state, and vice versa. The combination of the decrease in applied force and contact area for tensile residual stress and the increase in both for compressive stress can yield the residual stress-insensitive IIT hardness.

Suresh and Giannakipoulos [12] modeled equi-biaxial residual stress in IIT, assuming that hardness is constant and indentation force is dependent on surface residual stress, as in Fig. 1. This force-change was defined to be the differential contact force. Hydrostatic stress does not affect plastic defor-

*Corresponding author: juyoung@unist.ac.kr

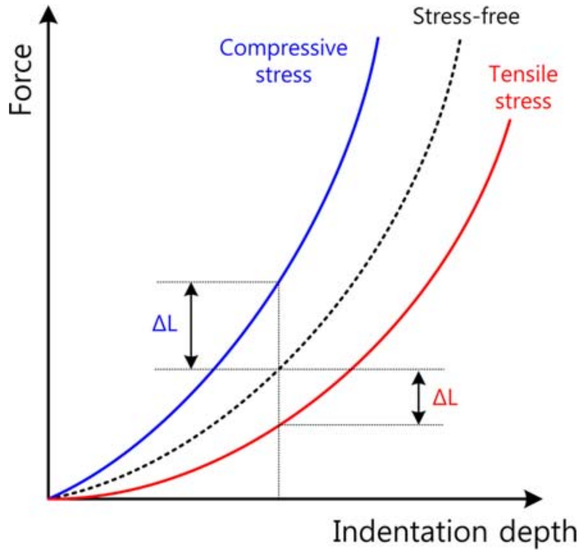

Fig. 1. Force-change in indentation force-depth curve by tensile and compressive surface residual stress.

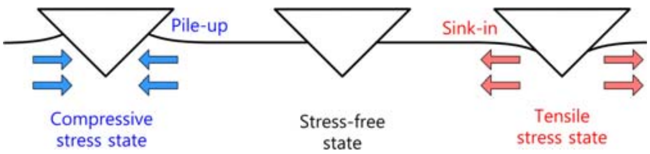

Fig. 2. Effect of residual stress on contact morphology in indentation loaded-state.

mation and equibiaxial stress was regarded as subtracting uniaxial stress from hydrostatic stress. Thus, the difference in force between the stressed and stress-free states ΔL is expressed by residual stress σ_{res} and contact area A_c. Lee and Kwon [1] expanded this model to non-equibiaxial residual stress in IIT; i.e., the residual stresses in the *x*- and *y*-directions are not identical, $\sigma^x_{res} \neq \sigma^y_{res}$. The residual stress for biaxial stress is given by

$$\overbrace{\begin{pmatrix} \sigma^x_{res} & 0 & 0 \\ 0 & \sigma^y_{res} & 0 \\ 0 & 0 & 0 \end{pmatrix} = \begin{pmatrix} \sigma^x_{res} & 0 & 0 \\ 0 & p\sigma^x_{res} & 0 \\ 0 & 0 & 0 \end{pmatrix}}^{\text{Biaxial stress}} =$$

$$\underbrace{\begin{pmatrix} \frac{(1+p)}{3}\sigma^x_{res} & 0 & 0 \\ 0 & \frac{(1+p)}{3}\sigma^x_{res} & 0 \\ 0 & 0 & \frac{(1+p)}{3}\sigma^x_{res} \end{pmatrix}}_{\text{Hydrostatic stress}} +$$

$$\underbrace{\begin{pmatrix} \frac{(2-p)}{3}\sigma^x_{res} & 0 & 0 \\ 0 & \frac{(2-p)}{3}\sigma^x_{res} & 0 \\ 0 & 0 & -\frac{(1+p)}{3}\sigma^x_{res} \end{pmatrix}}_{\text{Deviatoric stress}} \tag{1}$$

At a given p, the ratio of the residual stresses along the *x*- and *y*-directions $\sigma^y_{res}/\sigma^x_{res}$, the *zz*-component of the deviatoric stress and each residual stress for tensile residual stress are given as

$$\sigma^x_{res} = \frac{1}{\psi}\frac{3}{(1+p)}\frac{\Delta L}{A_c}$$
$$\sigma^y_{res} = p\sigma^x_{res} = p\frac{1}{\psi}\frac{3}{(1+p)}\frac{\Delta L}{A_c} \tag{2}$$

where ψ is the plastic constraint factor.

We propose a model to identify non-equibiaxial residual stress (i.e. p is not 1) using only IIT with a Knoop indenter, a four-sided pyramidal indenter with 7.11:1 ratio of two diagonals. Due to its geometric asymmetry, unlike Vickers and conical indenters with four-fold or axis-symmetric geometry, the Knoop indenter has been used to evaluate non-equibiaxial residual stress. A review of current models evaluating residual stress using Knoop IIT and a discussion of their limitations are given in the next sections. Unlike previous methods, here we evaluate the direction and amount of principal residual stress using only Knoop IITs. Also, we take into account the anisotropies in contact morphology and stress created by the asymmetric geometry of the Knoop indenter in our experimental and computational methods, making it possible to derive our theoretical model. The model is verified through a series of Knoop IITs on cruciform metallic samples where non-equibiaxial residual stress is controlled by a custom bending jig.

2. EVALUATION OF RESIDUAL STRESS BY KNOOP IIT

For non-equibiaxial stress, the force-change in the force-indentation depth curve depends on the planar orientation of the Knoop indentation. The Knoop indenter has twofold symmetry with a 7.11:1 ratio of long and short diagonals. To clarify the terminology in this study, we first assume an uniaxial stress state. For convenience, the residual stress along *x*-axis, σ^x_{res}, is assumed to be applied in parallel with the short diagonal of Knoop indentation and perpendicular to the long one, and σ^y_{res} is assumed to be applied 90° rotated from σ^x_{res}, as shown in Fig. 3. In the Knoop indentation force-indenta-

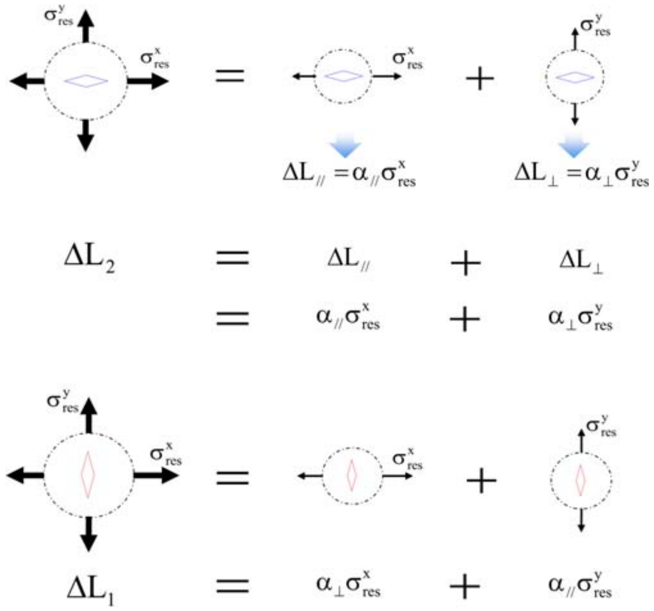

Fig. 3. Composition of force-changes in Knoop indentation as per principal directions.

tion depth curve, if the force changes by ΔL at a certain indentation depth h_t is generated by uniaxial residual stress σ^x_{res} compared to the stress-free curve, ΔL can be expressed by $\alpha_\perp \sigma^x_{res}$, where $\alpha_\perp$ is the conversion factor in Eq. (2). When a uniaxial residual stress σ^y_{res} is applied along the y-axis, the force change ΔL can similarly be expressed by $\alpha_{//}\sigma^x_{res}$. For non-equibiaxial stress, the force shift ΔL_1 in the force-indentation depth curve when the long diagonal is perpendicular to the x-axis is sum of the force-changes for two uniaxial stresses (Fig. 3), which is given by

$$\Delta L_1 = \alpha_\perp \sigma^x_{res} + \alpha_{//}\sigma^y_{res}. \tag{3-1}$$

The force-change ΔL_2 when the long diagonal of Knoop indentation is parallel to the x-axis is also given by

$$\Delta L_2 = \alpha_{//}\sigma^x_{res} + \alpha_\perp \sigma^y_{res}. \tag{3-2}$$

It is assumed that the x-axis is the principal direction of surface residual stress. Han *et al*. [13] verified Eqs. (3) based on experimental Knoop IITs on cruciform metal samples where surface residual stress is controlled by two-directional bending. They obtained the force-change ratio $\Delta L_2/\Delta L_1$ as

$$\frac{\Delta L_2}{\Delta L_1} = \frac{\dfrac{\alpha_{//}}{\alpha_\perp} + \dfrac{\sigma^y_{res}}{\sigma^x_{res}}}{1 + \dfrac{\alpha_{//}\sigma^y_{res}}{\alpha_\perp \sigma^x_{res}}} = \frac{\dfrac{\alpha_{//}}{\alpha_\perp} + p}{1 + \dfrac{\alpha_{//}}{\alpha_\perp}p} \tag{4}$$

where $\alpha_{//} / \alpha_\perp$ is defined as the conversion factor ratio. The

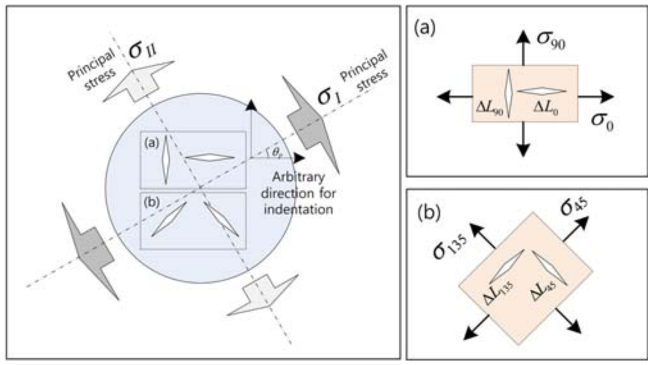

Fig. 4. Definition of force-changes ((a), (b)) in indentation force-depth curves and residual stress states when four Knoop IIT are carried out at four 45 degree rotated angles.

force-change ratio is a function of stress directionality p and the conversion factor ratio $\alpha_{//} / \alpha_\perp$; the conversion factor ratio is found to be 0.34 from experimental data [14]. They also showed that the conversion factor ratio is independent of material and indentation depth in their experiments, though the conversion factor depends on indentation depth.

If we measure ΔL_1 and ΔL_2 using Knoop IITs and use a constant of 0.34 for $\alpha_{//} / \alpha_\perp$, the stress directionality p can be determined from Eq. (4). However, we do not measure the actual values of σ^x_{res} and σ^y_{res}, but measure their ratio only. Additional IITs using indenters with geometric axis-asymmetry such as Vickers and conical indenters provide the sum of σ^x_{res} and σ^y_{res} experimentally, i.e. $\sigma^x_{res} + \sigma^y_{res} = \frac{3\Delta L}{\psi A_c}$ by Eq. (2), which makes it possible the measurement of quantitative values of σ^x_{res} and σ^y_{res} combined with the p value measured by Knoop IITs.

One condition for the algorithm in section 2.1 is that the principal direction is the x-axis. Kim *et al*. [15] suggested a model for evaluation of surface residual stress using Knoop IITs when the principal direction is not known. They suggested performing four Knoop IITs at four different angles, 0, 45, 90, and 135 degree rotated angles. In such cases, the principal direction is not known, so the first Knoop IIT angle is randomly chosen and 45 degrees between Knoop IITs is the relative angle. As shown in Fig. 4, the residual stress is expressed by sum of four directional stresses, σ^0_{res}, σ^{45}_{res}, σ^{90}_{res} and σ^{135}_{res}, and the force-changes in the Knoop indentation force-depth curves at four different angles are defined as ΔL_0, ΔL_{45}, ΔL_{90} and ΔL_{135}, respectively. We can use Eq. (4) to determine two stress-directionality p values from two pairs of force-changes, ΔL_0 and ΔL_{90}, and ΔL_{45} and ΔL_{135}. As in Eq. (4), two stress directionalities p' and p'' are described by

$$p' = \frac{\sigma^{90}_{res}}{\sigma^0_{res}} = \frac{\dfrac{\Delta L_0}{\Delta L_{90}} - \dfrac{\alpha_{//}}{\alpha_\perp}}{1 - \dfrac{\alpha_{//}\Delta L_0}{\alpha_\perp \Delta L_{90}}}, \tag{5-1}$$

$$p'' = \frac{\sigma_{res}^{135}}{\sigma_{res}^{45}} = \frac{\dfrac{\Delta L_{45}}{\Delta L_{135}} - \dfrac{\alpha_{//}}{\alpha_{\perp}}}{1 - \dfrac{\alpha_{//}}{\alpha_{\perp}}\dfrac{\Delta L_{45}}{\Delta L_{135}}}\,. \tag{5-2}$$

For the plane stress transformation, σ_θ is determined by rotation of the stress direction using Eqs. (6) and (7) [16];

$$\sigma_\theta = \frac{\sigma_{res}^{0} + \sigma_{res}^{90}}{2} + \frac{\sigma_{res}^{0} - \sigma_{res}^{90}}{2}\cos 2\theta + \tau_{xy}\sin 2\theta, \tag{6}$$

$$\tan 2\theta_p = \frac{2\tau_{xy}}{\sigma_{res}^{0} - \sigma_{res}^{90}}\,. \tag{7}$$

Using Eqs. (5), (6), and (7), the principal direction θ_p and the ratio of the principal residual stress P can be expressed as

$$\tan 2\theta_p = \frac{(1+p')(1-p'')}{(1-p')(1+p'')} \tag{8}$$

$$P = \frac{\sigma_2}{\sigma_1} = \frac{(1+p')\cos 2\theta_p - (1-p')}{(1+p')\cos 2\theta_p + (1-p')} \tag{9}$$

The advantage of this method is that we do not need to know the principal direction of the residual stress. By using Eqs. (8) and (9), the principal direction θ_p and ratio of principal residual stress P can be measured using four Knoop IITs at 45-degree rotated angles. However, as in the algorithm suggested in section 2.1, quantitative values of σ_{res}^{x} and σ_{res}^{y} are not measured by Eqs. (8) and (9). Additional IITs with indenters with geometric axis-asymmetry such as Vickers and conical indenters must be carried out to determine them quantitatively.

3. THEORETICAL MODELING

As defined in Eq. (1), the residual stress ratio p is given by

$$p = \frac{\sigma_{res}^{y}}{\sigma_{res}^{x}}, \tag{10}$$

where σ_{res}^{x} and σ_{res}^{y} are the x- and y-axis residual stresses, respectively. By substituting p into Eq. (2), we find the sum of the x- and y-axis residual stress as

$$\sigma_{res}^{x} + \sigma_{res}^{y} = \frac{3}{\psi}\frac{1}{A_c}\Delta L\,, \tag{11}$$

where Ψ is the plastic constraint factor. From the Knoop indentation model in Eq. (3), Eq. (11) becomes

$$\sigma_{res}^{x} + \sigma_{res}^{y} = \frac{1}{\alpha_{\perp} + \alpha_{//}}(\Delta L_1 + \Delta L_2)\,. \tag{12}$$

Setting Eqs. (11) and (12) equal to each other yields

$$\frac{3}{\psi}\frac{1}{A_c}\Delta L = \frac{1}{\alpha_{\perp} + \alpha_{//}}(\Delta L_1 + \Delta L_2)\,. \tag{13}$$

Indenters with axis-symmetric geometry such as Vickers and conical indenters were used to obtain quantitative residual stress values in previous work, as described above. We suggest using conical indenter with an angle satisfying the condition that ΔL in the conical IIT is equal to $\Delta L_1 + \Delta L_2$ in Knoop IIT. For IIT using this conical indenter,

$$\alpha_{\perp} + \alpha_{//} = \frac{\psi}{3}A_c\,. \tag{14}$$

We introduce the inverse of the conversion-factor ratio k, $\alpha_{\perp} / \alpha_{//}$, and combine it with Eq. (14) as

$$\alpha_{\perp} = \frac{\psi}{3}\cdot A_c \cdot \frac{k}{k+1}\,, \tag{15}$$

$$\alpha_{//} = \frac{\psi}{3}\cdot A_c \cdot \frac{k}{k+1}\,. \tag{16}$$

By introducing a trigonometric function, Eqs. (15) and (16) are generalized as

$$\alpha_\theta = \frac{\psi}{3}\cdot\frac{A_c}{2}\cdot\left(1 + \frac{k-1}{k+1}\cos 2\theta\right), \tag{17}$$

where θ is the angle between the long diagonal of Knoop indenter and an arbitrary reference line. If Ψ is taken as 3 [17] and the conversion-factor ratio k is regarded as 0.34 [13], we need to know contact area A_c in Knoop IIT to evaluate the conversion factors using Eqs. (15) and (16). Determining the A_c in Knoop IIT is discussed later below (Sec. 4).

For an unknown principal direction, the four force-shift values in Knoop indentation force-depth curves can be expressed in terms of conversion factors and principal residual stress components σ_I and σ_{II} as

$$\begin{pmatrix} \Delta L_1 \\ \Delta L_2 \\ \Delta L_3 \\ \Delta L_4 \end{pmatrix} = \begin{pmatrix} \alpha^{1}_{\theta_P+\theta_1} & \alpha^{2}_{\theta_P+\theta_1} \\ \alpha^{1}_{\theta_P+\theta_2} & \alpha^{2}_{\theta_P+\theta_2} \\ \alpha^{1}_{\theta_P+\theta_3} & \alpha^{2}_{\theta_P+\theta_3} \\ \alpha^{1}_{\theta_P+\theta_4} & \alpha^{2}_{\theta_P+\theta_4} \end{pmatrix} \begin{pmatrix} \sigma_I \\ \sigma_{II} \end{pmatrix}, \tag{18}$$

where θ_2 and θ_4 are $\theta_1 + 90^\circ$ and $\theta_2 + 90^\circ$, respectively. Combining the definition of the conversion factor and Eq. (17) gives

$$\Delta L_1 - \Delta L_2 = \left(\frac{\psi}{3}A_c\frac{k-1}{k+1}\cos 2(\theta_P + \theta_1)\right)(\sigma_I - \sigma_{II}) \tag{19}$$

$$\Delta L_3 - \Delta L_4 = \left(\frac{\psi}{3}A_c\frac{k-1}{k+1}\cos 2(\theta_P + \theta_3)\right)(\sigma_I - \sigma_{II}) \tag{20}$$

The difference between the principal residual stresses is given by Eqs. (19) and (20) as

$$\sigma_I-\sigma_{II}=\frac{\Delta L_1-\Delta L_2}{\frac{\Psi}{3}A_c\frac{k-1}{k+1}\cos 2(\theta_P+\theta_1)}=\frac{\Delta L_3-\Delta L_4}{\frac{\Psi}{3}A_c\frac{k-1}{k+1}\cos 2(\theta_P+\theta_3)}. \tag{21}$$

Subtractions of differences in force-shifts can be expressed in terms of θ as

$$\frac{\Delta L_3-\Delta L_4}{\Delta L_1-\Delta L_2}=\frac{\cos 2\theta_3-\tan 2\theta_P\sin 2\theta_3}{\cos 2\theta_1-\tan 2\theta_P\sin 2\theta_1}. \tag{22}$$

The principal direction θ_P is summarized as:

$$\tan 2\theta_P=\frac{(\Delta L_3-\Delta L_4)\cos 2\theta_1-(\Delta L_1-\Delta L_2)\cos 2\theta_3}{(\Delta L_3-\Delta L_4)\sin 2\theta_1-(\Delta L_1-\Delta L_2)\sin 2\theta_3}. \tag{23}$$

By taking θ_1 as 0° and θ_3 as 45°, Eq. (23) becomes

$$\tan 2\theta_P=-\frac{\Delta L_3-\Delta L_4}{\Delta L_1-\Delta L_2} \tag{24}$$

According to Eq. (24), the principal direction θ_P is determined by the force-change values in four Knoop IITs at four different angles: 0, 45, 90, and 135-degree rotated angles.

From Eq. (18), the sums of force-changes in Knoop IITs are

$$\Delta L_1+\Delta L_2=\left(\frac{\Psi}{3}A_c\right)\sigma_I+\left(\frac{\Psi}{3}A_c\right)\sigma_{II}, \tag{25}$$

$$\Delta L_3+\Delta L_4=\left(\frac{\Psi}{3}A_c\right)\sigma_I+\left(\frac{\Psi}{3}A_c\right)\sigma_{II}. \tag{26}$$

Eqs. (25) and (26) are rearranged as the sum of principal residual stresses as

$$\sigma_I+\sigma_{II}=\frac{\Delta L_1+\Delta L_2}{\frac{\Psi}{3}A_c}=\frac{\Delta L_3+\Delta L_4}{\frac{\Psi}{3}A_c}. \tag{27}$$

From Eqs. (19), (20), and (27), the principal residual stresses σ_I and σ_{II} are given by

$$\sigma_I=\frac{3}{\psi}\frac{1}{2A_c}\left\{(\Delta L_1+\Delta L_2)+\frac{k+1}{k-1}\frac{\Delta L_1-\Delta L_2}{\cos 2(\theta_P+\theta_1)}\right\}, \tag{28}$$

$$\sigma_{II}=\frac{3}{\psi}\frac{1}{2A_c}\left\{(\Delta L_1+\Delta L_2)-\frac{k+1}{k-1}\frac{\Delta L_1-\Delta L_2}{\cos 2(\theta_P+\theta_1)}\right\}. \tag{29}$$

Fixing θ_1 to be 0° yields

$$\sigma_I=\frac{3}{\psi}\frac{1}{2A_c}\left\{(\Delta L_1+\Delta L_2)+\frac{k+1}{k-1}\frac{\Delta L_1-\Delta L_2}{\cos 2\theta_P}\right\}, \tag{30}$$

$$\sigma_{II}=\frac{3}{\psi}\frac{1}{2A_c}\left\{(\Delta L_1+\Delta L_2)-\frac{k+1}{k-1}\frac{\Delta L_1-\Delta L_2}{\cos 2\theta_P}\right\}. \tag{31}$$

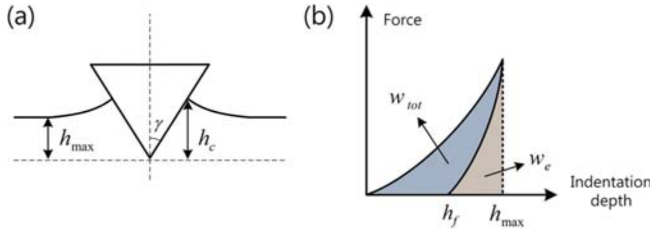

Fig. 5. (a) Schematics showing IIT parameters, maximum indentation depth h_{max}, contact depth h_c, (b) total work stored during loading W_{tot}, and work elastically-recoverd during unloading W_e.

Consequently, we can measure four force-change values by Knoop IITs, from which principal direction θ_P is also determined using Eq. (24). To determine the values of two principal residual stresses by Eqs. (30) and (31), we need to know the contact area A_c in Knoop IIT if Ψ is taken as 3 [17] and the conversion-factor ratio k is taken as 0.34 [13].

4. CONTACT AREA IN KNOOP IIT

For Vickers IIT, Kang *et al.* [8] suggested an indentation depth ratio f of

$$f=\frac{h_c}{h_{max}}, \tag{32}$$

where h_c and h_{max} are the contact depth and the maximum indentation depth in the loaded state, respectively, as shown in Fig. 5. They found the relation between the parameter f and indentation depths based on uniaxial tensile testing and IIT for 24 metal samples with a wide range of mechanical properties as

$$f=A\frac{h_{max}}{h_{max}-h_f}+B \tag{33}$$

where h_f is the final indentation depth as shown in Fig. 5 and A and B are dimensionless constants which were found to be 1.06 and 1.00, respectively. f is evaluated from indentation parameters h_{max} and h_f by Eq. (33), so that the true contact area A_c in the loaded state can be determined simply by an area function of the indenter that is a geometric relation between h_c and A_c. We extend their approach for Vickers IIT to Knoop IIT. Surface contact morphology for Knoop indentation with two-fold symmetry would be different from that for Vickers indenter with four-fold symmetry [8]. Maximum pile-up heights at short and long diagonals in optical microphotograph after unloading for Knoop indentation in previous study [14] are different each other. Surface profiling on residual indents such as AFM could be direct measurement of precise 3D surface morphology of Knoop indents as in previous research [18]. In this study, contact boundaries were so clear in optical microscope (OM) image that pile-up heights were determined from those OM images. Since the Knoop indenter is also geometrically self-similar, f for the

Table 1. Chemical compositions and mechanical properties of four cruciform metal samples

Materials	Chemical component (Fe bal.)	Elastic modulus (GPa)	Poisson's ratio	Yield strength (MPa)
S45C	0.45% C, 0.011% P, 0.07% Mn, 0.004% S and 0.03% Si	214	0.29	362
API X65	0.08% C, 0.019% P, 1.45% Mn, 0.003% S and 0.31% Si	210	0.29	490
Al6061	0.50% Si, 0.60% Mn, 4.35% Cu, 0.10% Cr, 0.15% Ti, 0.25% Zn, and 0.5% Fe (Al Bal.)	70	0.34	262
C10100	99.9% Cu	119	0.31	242

Knoop indenter can be related to the parameter $h_{max}/(h_{max}\text{-}h_f)$ as in Eq. (33). The effective cone angle of the Knoop indenter is greater than that of the Vickers indenter, so the constants in Eq. (33) are expected to differ from those for Vickers indenter.

To find the empirical relation between f and $h_{max}/(h_{max}\text{-}h_f)$ for Knoop IIT, we performed uniaxial tensile testing according to ASTM E8:09 [19] for 13 steels to measure yield strength and ultimate tensile strength, which are shown in Table 1. The elastic moduli in Table 1 were measured by an ultrasonic pulse-echo technique using a two-channel digital real-time oscilloscope. Steels with yield strengths ranging from 257 to 435 MPa and elastic moduli ranging from 190 to 223 GPa were selected. Knoop IIT was carried out using AIS3000 (Frontics Inc., Korea) with force resolution of 49 mN and displacement resolution of 0.1 μm. The loading and unloading rate was 0.3 mm/min, and a diamond Knoop indenter made by Synton MDP (Switzerland) was used. Machine compliance was pre-calibrated with a standard hardness block (Yamamoto Scientific Tool Laboratory Co., Chiba, Japan). The sample surfaces were finely polished with 1 μm diamond powder before IIT. Residual indents were observed by optical interferometer to evaluate contact area and contact depth.

For 13 steel materials, we found a good linear relation between f and $h_{max}/(h_{max}-h_f)$ (Fig. 6):

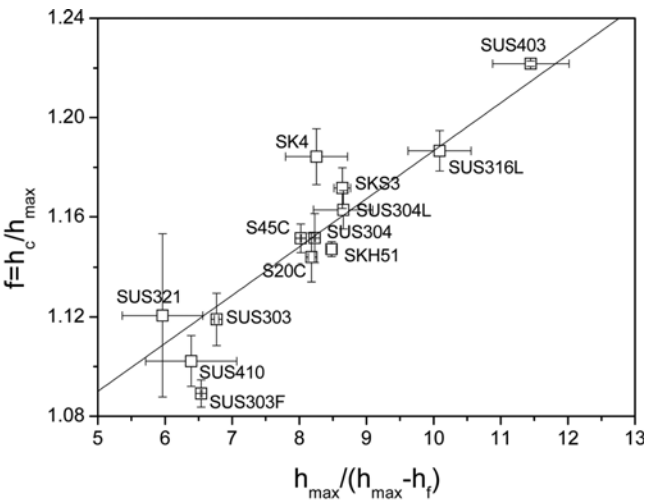

Fig. 6. Experimental relationship between the parameter f and $h_{max}/(h_{max}\text{-}h_f)$ for various ferrous metals.

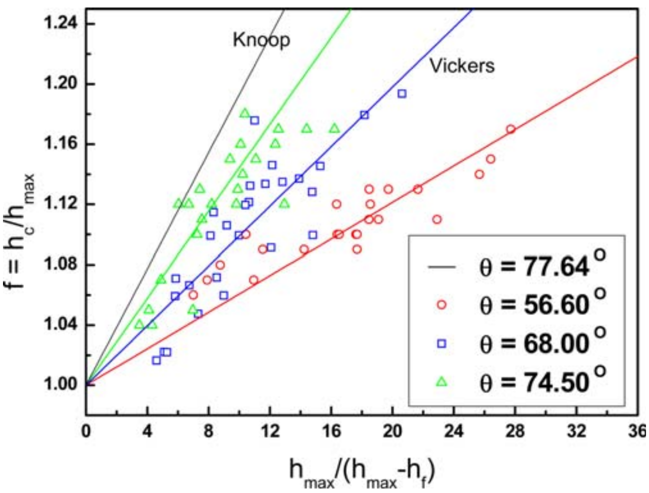

Fig. 7. Experimental relationship between the parameter f and $h_{max}/(h_{max}\text{-}h_f)$ for indenters with various effective cone angles. Each point was measured for different materials and blue open square points are cited from Kang *et al*'s work (2010).

$$f = 1.93 \times 10^{-2} \frac{h_{max}}{h_{max} - h_f} + 1.00 \,. \tag{34}$$

The value for the Vickers indenter of 1.06 in Eq. (33) and that for the Knoop indenter of 1.93×10^{-2} in Eq. (34) are quite different. The relations between f and $h_{max}/(h_{max}-h_f)$ for various indenters with different effective cone angles are presented in Fig. 7. The slope of linear fits in Fig. 7 tends to increase as the effective cone angle of indenters increases. The x-axis variable $h_{max}/(h_{max}-h_f)$ is related to W_{total}/W_e, where W_{total} is the total work stored by loading and W_e is the work elastically recovered during unloading (Fig. 5). Effect of indenter angle on pile-up height can be explained in terms of the hardness difference between the deformed zone, which is hardening by plastic deformation, and non-deformed zone, which is constraining the plastic deformation. Since a sharp indenter induces higher representative strain, the deformed zone is more strain-hardened, and thus the non-deformed zone cannot relatively constrain the deformed zone. Similarly, for an obtuse indenter, the relatively less strain-hardened deformed zone is constrained by non-deformed zone. Thus, pile-up height increases as effective cone angle increases, in agreement with the experimental results in Fig. 7. In previous results [8], the model for estimation of pile-up height during Vickers indentation describes experimental pile-up behavior for 24 metal samples including ferrous and Al, Mg, Cu, Ti, Ni alloys. Thus, this model would be expected for extending to other metallic materials, although only ferrous materials are selected for verifying this model in this study.

5. KNOOP IITs ON STRESSED SAMPLES

Four cruciform samples S45C, API X65, Al6061, and C10100 were prepared for Knoop IITs as shown in Fig. 8. Their chemical compositions and mechanical properties measured by uniaxial tensile testing and ultrasonic pulse-echo technique are presented in Table 2. The cruciform samples were annealed to remove any internal stress introduced during sample machining. The centers of the samples were finely mechanically polished for Knoop IITs. The surface residual stress-generating jig (Fig. 8) makes it possible to control non-equibiaxial surface residual stress by bending on two independent orthogonal axes. The amount of surface residual stress induced by the bending jig was measured by strain gages attached to the sample centers. According to the Tresca yield criterion, two orthogonal principal stresses were determined below each specimen's yield strength to prevent plastic deformation. Three stressed states, uniaxial, equibiaxial, and non-equibiaxial stresses, for the samples are summarized in Table 3. Figure 9 shows excellent linear relations between intentionally applied principal directions and principal directions measured by our Knoop IIT model.

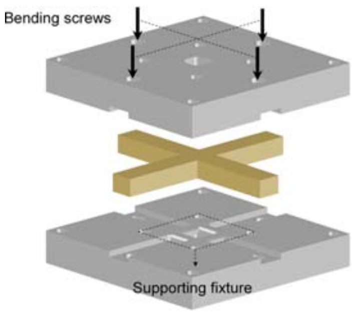

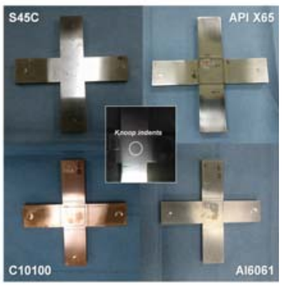

Fig. 8. Experimental set-up controlling surface residual stress in cruciform samples.

Table 3. Surface residual stress state applied in cruciform samples

Classification	Materials	Applied stress (MPa)		Principal direction (°)
		σ_I	σ_{II}	
Uniaxial	S45C	203	0	20
	API X65	127	0	30
	API X65	203	0	15
	Al6061	119	0	30
	C10100	187	0	30
Equi-biaxial	API X65	159	162	20
	API X65	130	125	40
	Al6061	83	82	30
	C10100	123	112	30
Biaxial	S45C	246	182	0
	API X65	219	115	60
	Al6061	124	59	30
	C10100	181	90	30

6. CONCLUSION

A Knoop IIT model was developed to evaluate surface residual stress. To apply this model, we need to know the plastic constraint factor of the material Ψ, the contact area in the Knoop indentation loaded states A_c, the conversion-factor ratio k and four force-changes in the indentation force-depth curve obtained at 45-degree rotated angles ΔL_0, ΔL_{45},

Table 2. Tensile properties of 13 ferrous metals

Type	Material	Elastic modulus (GPa)	Yield strength (MPa)	Tensile strength (MPa)
Ferritic steel	S20C	215.41	257.8	508.0
	S45C	211.88	362.7	774.2
	SK4	203.93	435.3	748.6
	SKH51	222.97	294.8	784.4
	SKS3	209.61	434.9	755.5
Stainless steel (austenitic)	STS303	206.49	326.3	1063.6
	STS303F	191.27	341.2	1167.0
	SUS304	189.97	321.3	1149.1
	SUS304L	202.68	338.7	1117.7
	SUS316L	198.36	304.7	950.7
	SUS321	197.42	317.4	894.8
Stainless steel (martensitic)	STS403	210.75	335.3	671.5
	STS410	214.54	366.5	669.0

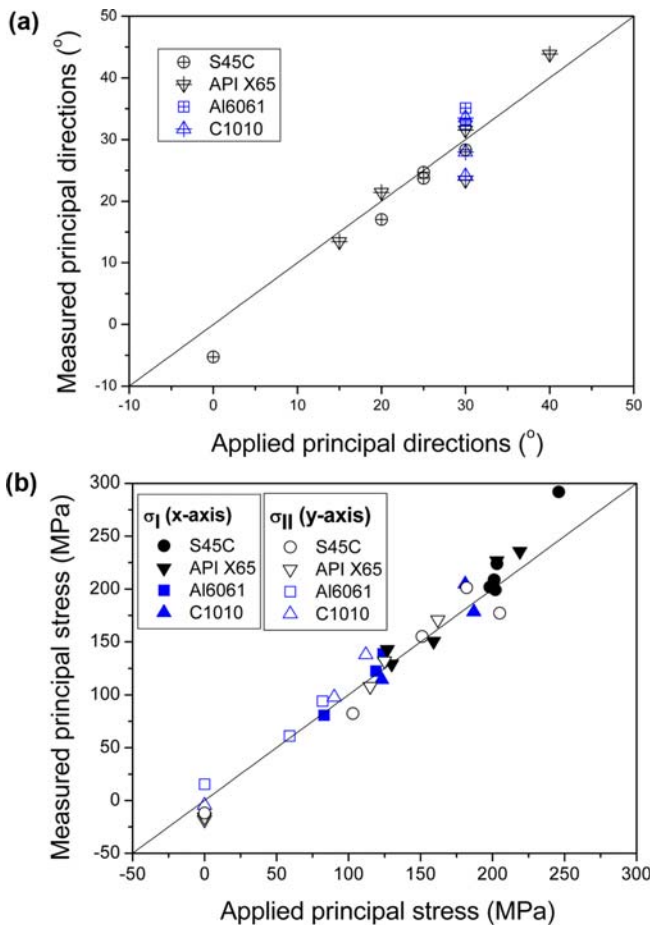

Fig. 9. Measured principal stresses and directions by proposed Knoop IIT model and applied principal stresses and directions ((a), (b)) in cruciform samples.

ΔL_{90}, ΔL_{135}. Ψ and k are taken as 3 and 0.34 from previous experimental studies. We found the related IIT parameters, maximum indentation depth h_{max} and final indentation depth h_f, and indentation depth ratio f taking into account the effect of pile-up during Knoop indentation, from which we determined contact area in Knoop IIT. The conversion factor was derived from experimental results and a previous indentation model, and we confirmed that it contained material and geometrical factors and the ratio of conversion factors. We designed an experimental setup to control surface residual stress by bending cruciform samples along two principal stress directions. Our Knoop IITs performed at 45-degree rotated angles on the bent cruciform samples showed excellent agreement between applied principal residual stresses/directions and the values obtained from our Knoop IIT model.

ACKNOWLEDGMENT

This work was supported by the 2011 Research Fund (1.110037.01) of UNIST (Ulsan National Institute of Science and Technology).

REFERENCES

1. Y.-H. Lee and D. Kwon, *Acta Mater*. **52**, 1555 (2004).
2. J.-I. Jang, *J. Ceram. Process. Res*. **10**, 391 (2009).
3. Y.-H. Lee, J. S. Park, Y.-i. Kim, and Y.-H. Huh, *Korean J. Met. Mater*. **53**, 90 (2015).
4. G. Sines and R. Carlson, *ASTM Bulletin 180*, **February**, 35 (1952).
5. A. Bolshakov, W. C. Oliver, and G. M. Pharr, *J. Mater. Res*. **11**, 760 (1996).
6. T. Y. Tsui, W. C. Oliver, and G. M. Pharr, *J. Mater. Res*. **11**, 752 (1996).
7. Y.-H. Lee and D. Kwon, *J. Mater. Res*. **17**, 901 (2002).
8. S. K. Kang, J. Y. Kim, C. P. Park, H. U. Kim, and D. Kwon, *J. Mater. Res*. **25**, 337 (2010).
9. J. Frankel, A. Abbate, and W. Scholz, *Exp. Mech*. **33**, 164 (1993).
10. W. R. Lafontaine, C. A. Paszkiet, M. A. Korhonen, and C.-Y. Li, *J. Mater. Res*. **6**, 2084 (1991).
11. A. V. Zagrebelny and C. B. Carter, *Scripta Mater*. **37**, 1869 (1997).
12. S. Suresh and A. E. Giannakopoulos, *Acta Mater*. **46**, 5755 (1998).
13. J. H. Han, J.-S. Lee, M.-J. Choi, G. Lee, K.-H. Kim, and D. Kwon, *Key Engineering*. **345-346**, 1125 (2007).
14. M.-J. Choi, S.-K. Kang, I. Kang, and D. Kwon, *J. Mater. Res*. **27**, 1 (2011).
15. Y.-C. Kim, M.-J. Choi, D. Kwon, and J.-Y. Kim, *Met. Mater. Int*. **21**, 850 (2015).
16. E. K. Girija, G. R. Sivakumar, S. Narayana Kalkura, P. Ramasamy, D. R. Joshi, and P. B. Sivaraman, *Mat. Chem. Phys*. **63**, 50 (2000).
17. D. Tabor, *The Hardness of Metals*, pp. 105-106, Oxford, New York (1951).
18. Y.-H. Lee, Y. Kim, Y.-C. Kim, J.-Y. Kim, and J.-I. Jang, *Met. Mater. Int*. **20**, 439 (2014).
19. ASTM E8 / E8M-15a, *Standard Test Methods for Tension Testing of Metallic Materials*, ASTM International, PA (2015).